RSC Advances

PAPER

View Article Online
View Journal | View Issue

Check for updates

Cite this: *RSC Adv.*, 2018, **8**, 176

Schiff base-functionalized mesoporous silicas (MCM-41, HMS) as Pb(II) adsorbents

Daniela F. Enache,[a] Eugenia Vasile,[a] Claudia Maria Simonescu,[a] Daniela Culita,[b] Eugeniu Vasile,[a] Ovidiu Oprea,[a] Andreea Madalina Pandele,[a] Anca Razvan,[a] Florina Dumitru *[a] and Gheorghe Nechifor[a]

Received 10th November 2017
Accepted 12th December 2017

DOI: 10.1039/c7ra12310h

rsc.li/rsc-advances

Three Schiff base-functionalized mesoporous silicas: MCM-41@salen, HMS-C12@salen and HMS-C16@salen have been synthesized by a post-synthetic grafting strategy and their sorption capacities toward Pb(II) from synthetic aqueous solutions have been assessed. FTIR spectra, TG/DSC analyses, X-ray powder diffraction, X-ray photoelectron spectroscopy (XPS), N_2 adsorption isotherms and HRTEM micrographs were used to characterize the novel functionalized mesoporous silicas. The novel adsorbents have been tested for their capability in the remediation of synthetic aqueous systems containing Pb(II). The Langmuir maximum values of sorption capacities of these adsorbents toward Pb(II) are: 138.88 mg Pb(II) per g MCM-41@salen, 144.92 mg Pb(II) per g HMS-C12@salen, and 181.81 mg Pb(II) per g HMS-C16@salen, therefore, the functionalized silicas (MCM-41@salen, HMS-C12@salen, HMS-C16@salen) could be used as effective adsorbents of Pb(II) ions from wastewater.

1. Introduction

Modifications by post-grafting strategy of the silica surface of MCM-41/HMS materials have been widely studied and numerous organofunctionalized materials for selective and advanced separation processes have been obtained.[1–6] Conventional routes of silica surface modification by chemical treatment methods are based on the reaction between the surface silanol groups and commercial silane coupling agents as precursors for immobilization of organic molecules. One of the most used silylation agents is 3-aminopropyl trimethoxysilane (APTES)[7,8] and the amount of organic moieties obtained by grafting of APTES is usually 1–1.5 mmol g_{solid}^{-1}.[4,9]

Therefore, the post-grafting strategy represents a simple route for anchoring the functional chelating ligands into the pores and, consequently, affords the obtaining of a plethora of organo-functionalized mesoporous silicas that could be used as adsorbents of toxic materials.

Among these materials, those having grafted salicylaldoxime (salen) ligands represent efficient sorbents and they were extensively used for remediation of wastewater containing heavy metal ions. Soliman *et al.*[10] obtained mono- and bis-salicylaldehyde Schiff base ligands grafted on silica surface in a three-step approach: silanization of silica surface with 3-chloropropyltrimethoxysilane, replacing the chlorine leaving group with amino-group from diethylenetriamine, followed by the condensation with salicylaldehyde. The as-prepared hybrid materials show high selectivity in extraction of Cu(II) (metal uptake capacity 0.957 mmol g^{-1}) and Fe(III) (0.643 mmol g^{-1}). In a similar approach, Kim *et al.*[11] synthesized a chiral salen-mesoporous MCM-41 material that has been further involved in Mn(III) coordination, thus providing a catalyst for styrene epoxidation with high level of enantioselectivity. Sarkar *et al.*[12] demonstrated that preconcentration of Cu(II), Zn(II), Co(II), Fe(III) and Ni(II) in water could be highly effective by using the silica gel modified with salicylaldoxime. Parvulescu *et al.*[13,14] reported the preparation of *n*-propyl-salicylaldimine modified SBA-15/SBA-16 mesoporous silicas and the study of their efficiency in sorption of heavy metal ions, they found out that adsorption capacities decrease within the following series: Cu(II) > Co(II) ⋙ Mn(II). Functionalized SBA-15 mesoporous silica particles, bearing ethylenediaminepropyl-salicylaldimine and *N*-propylsalicylaldimine Schiff base ligands, were examined as adsorbents in solid phase extraction (SPE) of uranyl (UO_2^{2+}) ions from water.[15] The maximum adsorption capacities determined for these adsorbents were 105.3 and 54 mg uranyl per g adsorbent, respectively. Chen *et al.*[16] prepared a Schiff base immobilized hybrid mesoporous silica membrane for the detection of Cu(II) by immobilizing 4-chloro-2-[(propylimino)methyl]-phenol (4-chloro-salen) onto the pore surface of mesoporous silica embedded in the pores of an anodic alumina membrane. The detection limit for Cu(II) was 0.8 μM. Gao *et al.*[17] previously used the same ligand to obtain (*via* a self-assembly process) a mesoporous silica material SBA-15–APTES–4-chloro-2-

---

[a] *Politehnica University Bucharest, 1 Polizu st., 011061, Bucharest, Romania. E-mail: florina.dumitru@upb.ro*

[b] *"Ilie Murgulescu" Institute of Physical Chemistry, Splaiul Independentei 202, Bucharest, Romania*

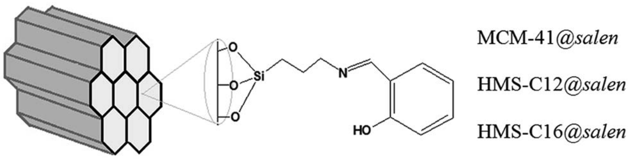

Fig. 1 Schematic representation of mesoporous adsorbents: MCM-41@salen, HMS-C12@salen (C12 – dodecylamine), HMS-C16@salen (C16 – hexadecylamine).

[(propylimino)methyl]-phenol, as Zn(II)-sensitive fluorescent chemosensor.

Porous silica functionalized with *N*-propylsalicylaldimine was used for separation and preconcentration of Cu(II), Cr(III, VI), Cd(II), Pb(II) and Mn(II, VII) from natural waters.[18]

In this work, we describe the obtaining of ordered mesoporous silicas (MCM-41 and HMS type) with hemisalen Schiff base grafted onto the silica surface (Fig. 1).

The functionalization of the MCM-41/HMS silicas has been carried out by heterogeneous grafting method: first, the silylating agent (3-aminopropyl)triethoxysilane (APTES) reacted with the surface hydroxyl groups to give the amino-functionalized silica (MCM-41@APTES, HMS-C12@APTES, HMS-C16@APTES) and then the salicylaldehyde was covalently attached (MCM-41@salen, HMS-C12@salen, HMS-C16@salen).

FTIR spectra, TG/DSC analyses, X-ray powder diffraction, X-ray photoelectron spectroscopy (XPS), N_2 adsorption isotherms and HRTEM micrographs were used to characterize the novel functionalized materials.

The obtained mesoporous adsorbents have been assessed for the effectiveness in the remediation of synthetic aqueous systems containing Pb(II). The factors that influence the sorption behavior have been studied: heavy metal ion concentrations, pH of solution, contact time, as well as the adsorption isotherms.

2. Experimental

2.1. Techniques and materials

All the raw materials were commercially available and used as received.

FTIR vibrational spectra were registered with a Bruker Tensor 27 spectrophotometer equipped with one ATR sampling unit, in the wavenumbers range of 500–4000 cm^{-1}.

Thermal analysis was carried out with a Netzsch 449C STA Jupiter. Samples were placed in open alumina crucible and heated with 10 degrees per min from room temperature to 900 °C, under the flow of 20 mL min^{-1} dried air. An empty Al_2O_3 crucible was used as reference.

Powder X-ray diffraction (PXRD) patterns were registered on a Panalytical X'PERT PRO MPD diffractometer with graphite monochromatized CuK_α radiation ($\lambda = 1.54$ Å). The samples were scanned in the Bragg angle, 2θ range of 2–10° and step size of 0.013°.

For TEM and HRTEM analysis we used TECNAI F30 G^2 high-resolution transmission electron microscope operated at an accelerating voltage of 300 kV device. The samples have been prepared by dispersing the particles by ultrasonication in methanol and subsequently collected into a holey carbon-coated TEM support grid.

The N_2 adsorption/desorption isotherms for pore size distribution and BET specific surface measurements were recorded on a Micromeritics ASAP 2020 analyzer. Before analysis the samples were outgassed at 120 °C for at least 6 hours under vacuum.

X-ray photoelectron spectroscopy (XPS) data were registered on a Thermo Scientific K-Alpha device, fully integrated, with an aluminium anode monochromatic source (1486.6 eV). The survey spectra were registered using a pass energy of 200 eV at bass pressure of 2×10^{-9} mbar.

The pH measurements were taken with Agilent 3200P pH Meter. Batch equilibrium experiments on the GFL 3031 Incubating Shaker at 150 rpm were performed. Atomic Absorption Spectrometry on contrAA® 300 Analytik Jena Atomic Absorption Spectrometer was applied to determine Pb(II) ions concentration in aqueous solutions. All the equilibrium experiments were carried out by contacting 0.025 g of adsorbent with 25 mL of synthetic aqueous solution of 100 mg L^{-1} Pb(II), at room temperature, for 24 hours and 150 rpm. After reaching the equilibrium, the Pb(II) concentrations in filtrate samples have been determined by AAS.

2.2. Preparation of functionalized mesoporous silicas

2.2.1. MCM-41. MCM-41 mesoporous silica has been prepared by using cetyltrimethylammonium bromide (CTAB) as structure-directing agent and tetraethoxysilane (TEOS) as sol precursor to form silica mesopores, according to an adapted literature procedure.[19]

The reaction mixture was composed of 1.0CTAB : 9.21TEOS : 2.55NaOH : $4857H_2O$ (molar ratios). CTAB and NaOH formed the initial reaction mixture in water that was further heated at 80 °C for 30 min. TEOS was added at pH 12. After 2 h at 80 °C, white solid MCM-41 precipitated. The product was filtered off, washed with large volumes of water and methanol and dried in oven at 105 °C for 6 h. The surfactant (CTAB) has been removed by thermal treatment at 550 °C for 6 h.

2.2.2. HMS-C12 and HMS-C16. Hexagonal mesoporous silicas (HMS) have been synthesized following the procedure described by Tanev and Pinnavaia:[20] HMS-C12 and HMS-C16 were prepared by hydrolysis of TEOS in presence of $C_nH_{2n+1}NH_2$ primary amines as structure-directing agents ($n = 12$ for HMS-C12 and $n = 16$ for HMS-C16, respectively), water and ethanol. For each material, the molar ratio in the reaction mixture was: 1.0TEOS : $0.27C_nH_{2n+1}NH_2$: $9.09C_2H_5OH$: $29.6H_2O$.

The syntheses were accomplished at room temperature, the reaction mixtures were aged for 24 h and the obtained HMS solids were recovered by filtration, washed with deionized water and dried at 105 °C for 6 h. The primary amines ($C_{12}H_{25}NH_2$, dodecylamine and $C_{16}H_{33}NH_2$, hexadecylamine) have been removed by calcination in air at 630 °C for 4 h.

2.2.3. APTES modification of mesoporous silicas: MCM-41@APTES, HMS-C12@APTES, HMS-C16@APTES. Following a general procedure, the mesoporous silicas have been derivatized with 3-aminopropyl triethoxysilane, APTES, in toluene, as follows: 3 g of mesoporous silica (MCM-41, HMS-C12 or HMS-C16, dried at 160 °C for 5 h, under vacuum) and APTES (2.5 mL) in toluene (100 mL) were refluxed for 24 h, under inert atmosphere.

In each case, the resulting silica (MCM-41@APTES, HMS-C12@APTES or HMS-C16@APTES) was collected by centrifugation, then washed with toluene to remove the adsorbed APTES, filtered and dried at 80 °C, for 24 h.

2.2.4. Hemisalen ligand formation on the MCM-41@APTES, HMS-C12@APTES and HMS-C16@APTES surfaces. In this step, the condensation reactions between salicylaldehyde and the free amino group (from APTES grafted onto silica surface) have been carried out in methanol, and MCM-41@salen, HMS-C12@salen and HMS-C16@salen have been obtained. The molar ratio for APTES-derivatized silica (MCM-41@APTES, HMS-C12@APTES or HMS-C16@APTES) and salicylaldehyde was 1 : 30. After continuous stirring at room temperature for 5 h, the colorless reaction mixture (both liquid and solid phases) became yellow. The yellow solid was filtered, extensively washed with methanol and finally dried under reduced pressure.

3. Results and discussion

3.1. FTIR spectra

In the FTIR spectra (Fig. 2, Table 1) of functionalized silica materials, stretching vibrational bands specific to silica network and to organic moieties (*i.e.* the surfactant or the covalently bonded aminopropylsiloxane linker/salen ligands) are present. The strongest signals in FTIR spectra are assigned to Si–O–Si 1100 cm^{-1} corresponding with the silica network formed as a result of hydrolysis/condensation reactions between the silica precursors.

Peaks characteristic to the newly formed imine bonds (C═N) appeared in MCM-41@salen, HMS-C12@salen, and HMS-C16@salen FTIR spectra at ~1635 cm^{-1}, indicative for the salen-type ligands grafted onto silica surface.

3.2. XPS data

XPS scans (Fig. 3) carried out on MCM-41@salen, HMS-C12@salen, HMS-C16@salen revealed that they have as constitutive elements: C–C 1s, N–N 1s, O–O 1s, and Si–Si 2p with the corresponding binding energies presented in Table 2. The C–C 1s, N–N 1s are clearly resulted from the organic moieties grafted onto silica surface.

The atomic contents (converted in weight percents, Table 2) suggest that about 50% of the APTES moieties (for organic content: APTES = C_3H_8N and APTES + salicylaldehyde = $C_{10}H_{12}N$)

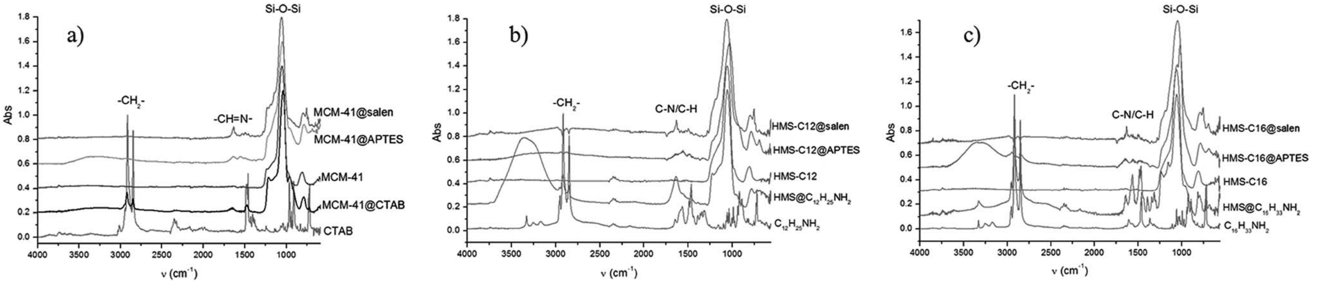

Fig. 2 FTIR spectra of (a) CTAB, MCM-41@CTAB, MCM-41, MCM-41@APTES, MCM-41@salen; (b) $C_{12}H_{25}NH_2$, HMS@$C_{12}H_{25}NH_2$, HMS-C12, HMS-C12@APTES, HMS-C12@salen; (c) $C_{16}H_{33}NH_2$, HMS@$C_{16}H_{33}NH_2$, HMS-C16, HMS-C16@APTES, HMS-C16@salen.

Table 1 Characteristic stretching/deformation vibration bands in FTIR spectra of synthesized silicas

Compound/material	ν(N–H)	ν(CH$_{2as/sym}$)	ν(C═N)	ν(C–C), ν(C–N)	δ(CH$_2$)/δ(NH$_2$)	δ(N$^+$–CH$_3$)	ν(Si–O–Si)
CTAB	—	2913/2848	—	962/912	1461, 1475/—	1488	—
MCM-41@CTAB	—	2923/2852	—	962/910	1477, 1467/—	1490	1039
MCM-41	—	—	—	—	—	—	1053
MCM-41@APTES	3351 (br)	2926	—	—	—/1643, 1551	—	1051
MCM-41@salen	—	2927	1648–1635	964/898	1459, 1498	—	1058
$C_{12}H_{25}NH_2$	3328 (s)	2916/2847	—		1464, 1487/1649, 1567	—	—
HMS@$C_{12}H_{25}NH_2$	3350 (br)	2922/2853	—	960/888	1467/1641	—	1056
HMS-C12	—	—	—	—	—	—	1058
HMS-C12@APTES	—	2942/2881	—	923	1489, 1457/1652, 1559		1032
HMS-C12@salen	—	2922/2852	1633	—	1492, 1461	—	1065
$C_{16}H_{33}NH_2$	3331 (s)	2917/2848	—	973/924	1471, 1451	—	—
HMS@ $C_{16}H_{33}NH_2$	3324 (s)	2918/2850	—	955	1485, 1469/1642, 1565	—	1058
HMS-C16	—	—	—	—	—	—	1060
HMS-C16@APTES	3330 (br)	2947/2834	—	—	1452/1649, 1564	—	1055/1018
HMS-C16@salen	—	2920/2851	1635		1457/—	—	1047

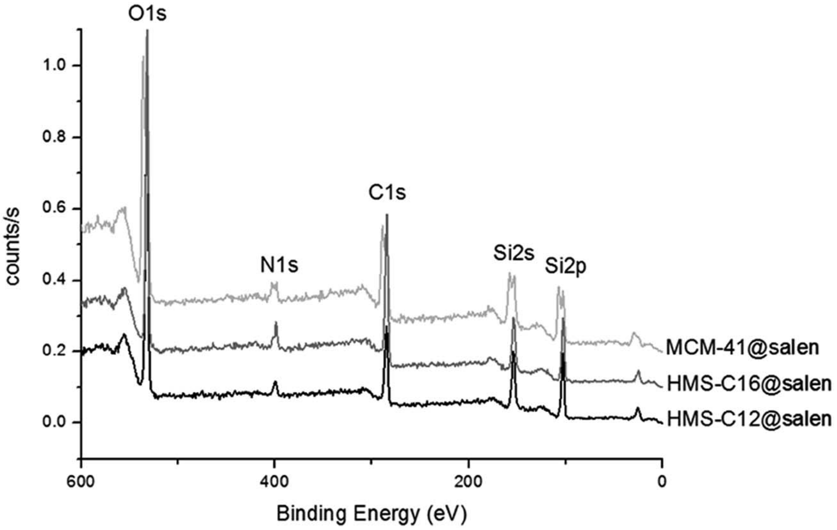

Fig. 3 XPS spectra of MCM-41@salen, HMS-C12@salen, HMS-C16@salen (the spectra were normalized and shifted on the *y* axis).

Table 2 XPS binding energies for MCM-41@salen, HMS-C12@salen, HMS-C16@salen and elemental compositions of mesoporous silicas

	Binding energy values (eV)				Found (% wt)			
Mesoporous silicas	C–C 1s	N–N 1s	Si–Si 2p	O–O 1s	C	N	Si	O
MCM-41@salen	285.00	400.20	103.06	532.26	23.54	3.90	37.82	34.73
HMS-C12@salen	285.48	399.75	103.44	532.97	19.80	3.43	39.15	37.62
HMS-C16@salen	284.89	399.02	102.91	532.21	30.47	5.33	35.23	28.97

have been reacted to form a bond between the amino group (APTES) and the carbonyl group (salicylaldehide). Supposing that all the nitrogen and carbon content comes from the APTES and APTES + salicylaldehyde, we found that the theoretical carbon-to-nitrogen (C : N) mass ratio is 5.57 : 1 for 1 : 1 APTES : APTES + salicylaldehyde and this ratio agrees fairly well with the experimental ones (6.03 : 1 for MCM-41@salen, 5.77 : 1 for HMS-C12@salen and 5.72 : 1 for HMS-C16@salen, respectively).

3.3. Thermal analysis

TG-DSC analyses (Fig. 4 and 5) also support the conclusions drawn from the FTIR and XPS spectra.

All the as-prepared mesoporous silicas have similar thermal behavior with three main mass loss peaks, illustrated by TG curves: volatilization of the adsorbed solvent (below 100 °C), decomposition of organic fragments grafted in the silica pores

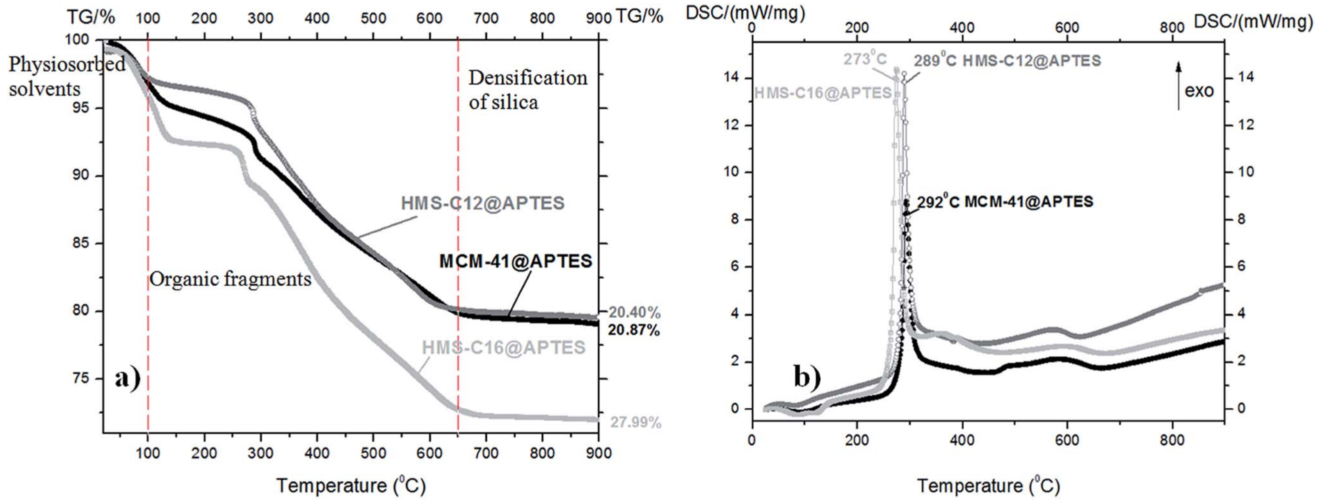

Fig. 4 (a) TG curves and (b) DSC curves of the silanized mesoporous silicas: MCM-41@APTES, HMS-C12@APTES and HMS-C16@APTES.

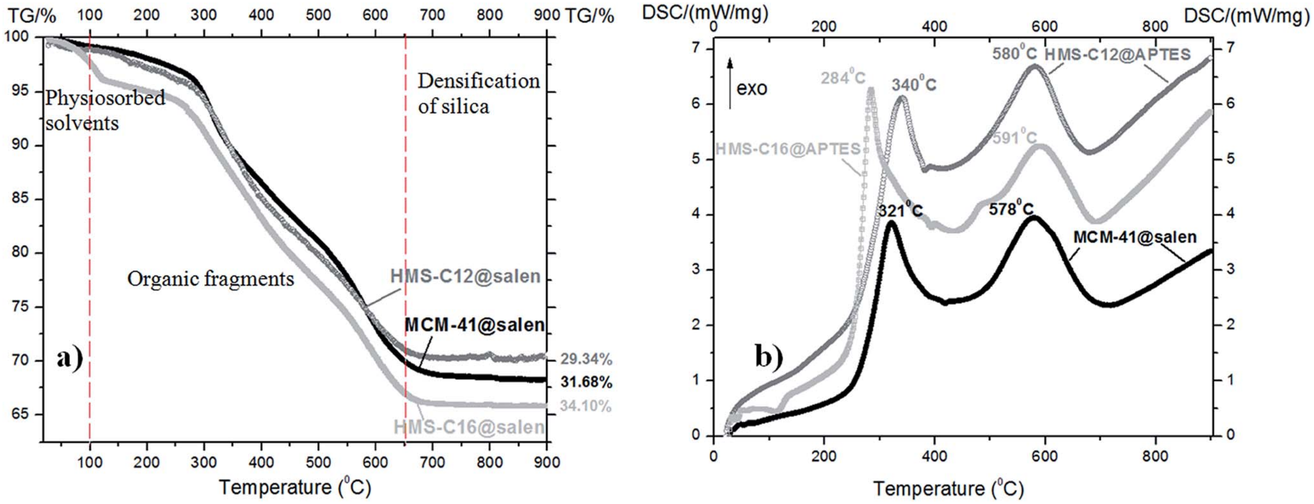

Fig. 5 (a) TG curves and (b) DSC curves of the functionalized mesoporous silicas: MCM-41@salen, HMS-C12@salen and HMS-C16@salen.

(100–650 °C), and densification of the silica matrix (above 650 °C up to 900 °C).

The DSC curves are very similar in shape for all three organofunctionalized silicas:

- they present one strong exothermic effect centered at 292 °C for MCM-41@APTES, at 289 °C for HMS-C12@APTES and at 273 °C for HMS-C16@APTES, respectively.
- two strong exothermic effects: first effect is centered at 321 °C for MCM-41@salen, at 340 °C for HMS-C12@salen and 284 °C for HMS-C16@salen, respectively, and the second effect occured at 578 °C (MCM-41@salen), at 580 °C (HMS-C12@salen), and at 591 °C (HMS-C16@salen), respectively. The former effect could be assigned to the decomposition of organic ligand grafted onto silicas and the latter to the removal of the residual combustion compounds originated from the decomposition of organic part.

The TG-DSC data are consistent with the results of as-prepared samples XPS measurements. The largest mass loss was found for HMS-C16@salen, similarly to the XPS results where the highest organic content was also found for HMS-C16@salen.

3.4. Powder XRD

The XRD patterns of all synthesized silicas show the hexagonal ordered porous structure (Fig. 6), with the following particularities:

– MCM-41 (Fig. 6a, Table 3) exhibits one sharp (100) reflection at $2\theta = 2.16^\circ$ and additional Braggs peaks indexed as (110), (200), and (210) reflections characteristic for hexagonal symmetry (*P6mm* space group).[21] In comparison with the XRD diagram of the parent MCM-41 subjected to post-synthetic organofunctionalization, MCM-41@salen exhibits the sharp reflection 2θ (100) at 2.30°, but only very weak peaks at $2\theta = 4.60^\circ$ (200) and $2\theta = 6.09^\circ$ (210), a common feature of MCM-41 silicas with organic ligands incorporated into the pore channels.

– HMS-C12 (Fig. 6b, Table 3) and HMS-C16 (Fig. 6c, Table 3) exhibit a single low angle reflection (100) at $2\theta = 2.03^\circ$ (HMS-C12) and $2\theta = 1.76^\circ$ (HMS-C16) indicative of the average pore–pore correlation distance in their hexagonal lattices.[20] For these silicas, it is assumed that the framework mesopores are wormholelike with some spatial orientation of the pores within the particles, *i.e.* local hexagonal symmetry. As the alkylamines used as surfactants are of C12 (HMS-C12) and C16 (HMS-C16)

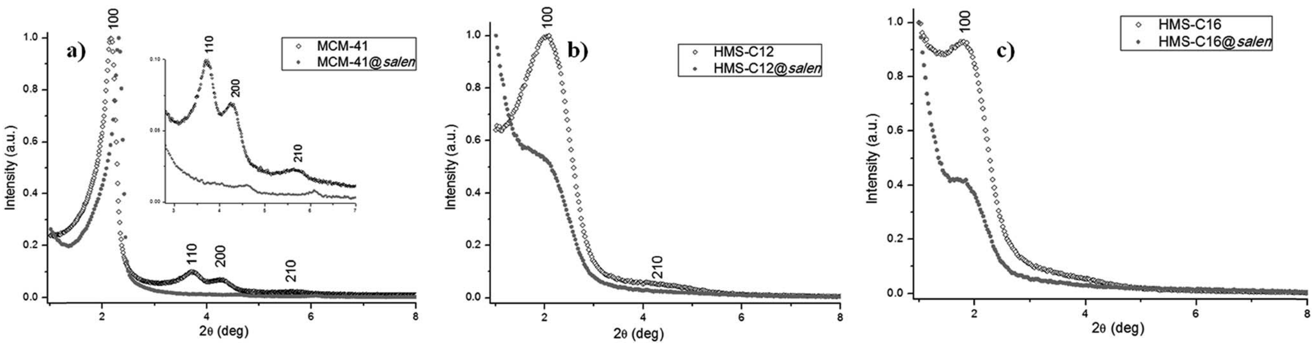

Fig. 6 XRD patterns for the synthesized mesoporous silicas: (a) MCM-41, MCM-41@salen; inset graph: enlargement of the XRD pattern with diffraction planes indices; (b) HMS-C12, HMS-C12@salen; (c) HMS-C16, HMS-C16@salen.

Table 3 Structural properties of the prepared mesoporous silicas

Miller indices			MCM-41, $a_0 = 4.724$ nm		MCM-41@salen, $a_0 = 4.424$ nm		HMS-C12, $a_0 = 5.031$ nm		HMS-C12@salen, $a_0 = 5.283$ nm		HMS-C16, $a_0 = 5.783$ nm		HMS-C16@salen, $a_0 = 5.899$ nm	
h	k	l	2θ (°)	d_{hkl} (nm)	2θ (°)	d_{hkl} (nm)	2θ (°)	d_{hkl} (nm)	2θ (°)	d_{hkl} (nm)	2θ (°)	d_{hkl} (nm)	2θ (°)	d_{hkl} (nm)
1	0	0	2.16	4.09	2.30	3.83	2.03	4.36	1.93	4.57	1.76	5.01	1.73	5.11
1	1	0	3.71	2.38	—	—	—	—	—	—	—	—	—	—
2	0	0	4.26	2.08	4.60	1.92	—	—	—	—	—	—	—	—
2	1	0	5.82	1.52	6.09	1.45	4.42	2.00	—	—	—	—	—	—

chain lengths, the position of the single (100) reflection is present at lower 2θ value for HMS-C16, indicating the increase of the average distance between the pore centres. Hexadecylamine, $C_{16}H_{33}NH_2$, as structure-directing agent for HMS-C16, has a longer alkyl chain length and it afforded a silica material with larger framework mesopore sizes (HMS-C16: $d_{100} = 5.01$ nm *vs.* HMS-C12: $d_{100} = 4.36$ nm).

For HMS-C12@salen (Fig. 6b, Table 3) and HMS-C16@salen (Fig. 6c, Table 3), the post-synthetic grafting of organic ligands caused a significant decrease in the (100) peak intensity and the complete lack of the higher order Bragg reflections in their diffraction patterns (Fig. 6b and c), both features indicate the incorporation of organic moieties into the pore channels of the HMS-C12 and HMS-C16 materials, without the collapse of the pore structure. In conclusion, the pore channels in all HMS silicas prepared by us show uniform framework mesopore distribution with short range hexagonal order. The lack of longer range order is explained by the relatively weak hydrogen-bonding interactions that operate in the neutral (alkylamine:-TEOS) assembly process.

The values of the corresponding unit cell parameter a_0 were calculated using the formula: $a_0 = 2d_{100}/3^{1/2}$, where d_{100} represents the *d*-spacing value of the (100) diffraction peak in XRD patterns of the samples.

3.5. High-resolution transmission electron microscopy (HRTEM)

In addition to XRD patterns, HRTEM images (Fig. 7) further confirm the ordered structures of MCM-41@salen (Fig. 7A), HMS-C12@salen (Fig. 7B) and HMS-C16@salen (Fig. 7C).

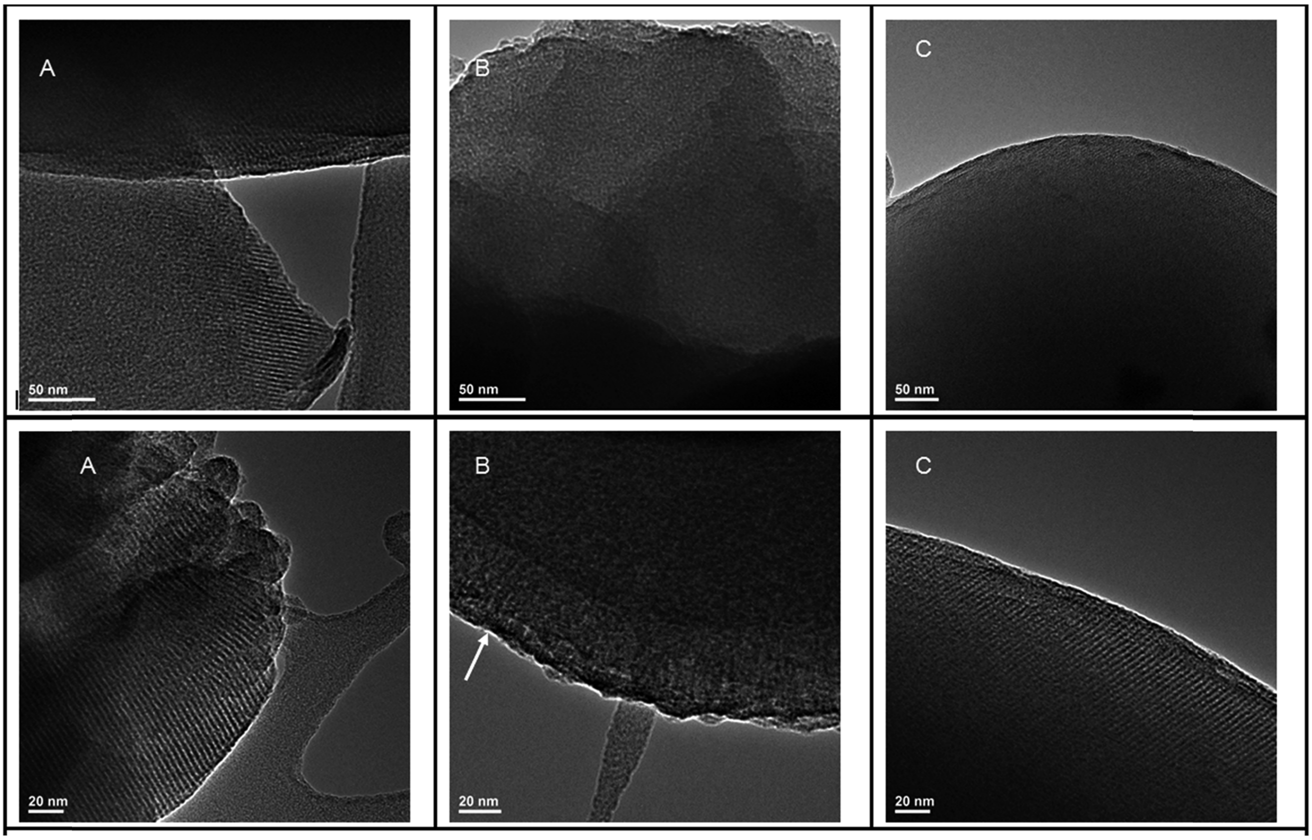

Fig. 7 HRTEM images (scale bars 50 nm and 20 nm) for (A) MCM-41@salen; (B) HMS-C12@salen; (C) HMS-C16@salen.

Table 4 Textural properties of MCM-41, MCM-41@salen, HMS-C12, HMS-C12@salen, HMS-C16, and HMS-C16@salen samples

Sample	d_{100} (nm) XRD	a_0 (nm)	Pore volume (cm^3 g^{-1})	d_{pore} (nm)	S_{BET} (m^2 g^{-1})
MCM-41	4.09	4.724	0.733	2.75	964
MCM-41@salen	3.83	4.424	0.029	—	27
HMS-C12	4.36	5.030	0.759	3.14	694
HMS-C12@salen	4.57	5.283	0.098	3.67	134
HMS-C16	5.01	5.783	0.949	4.06	653
HMS-C16@salen	5.11	5.899	0.053	—	8

MCM-41@salen exhibits typical MCM-41 highly ordered mesoporous structure, whose hexagonal lattice has been preserved after the functionalization, in accord with the corresponding XRD data.

HRTEM images for HMS-C12@salen show uniform wormholelike channels (mesopores) distributed homogeneously throughout the bulk phase over a short range hexagonallike order (see arrow, Fig. 7B). HRTEM micrograph of HMS-C16@salen sample (Fig. 7C) revealed that the mesoporous framework is better-defined than that of HMS-C12@salen, the hexagonal order being comparable to the MCM-41@salen structure. It is known that for longer alkyl chains (number of carbon atoms > 12), the structure of the HMS template changes from rod-like micelles to lamellar micelles.[20,22,23]

3.6. Nitrogen adsorption–desorption isotherms

Using Brunauer–Emmett–Teller (BET) and Barrett–Joyner–Halenda (BJH) methods, the specific surface area and the average pore diameter of the samples have been calculated. The structural parameters of MCM-41, MCM-41@salen, HMS-C12, HMS-C12@salen, and HMS-C16, HMS-C16@salen samples (pore volume, pore diameter and BET surface area) were summarized in Table 4. The N_2 sorption isotherms for the synthesized silicas: MCM-41, MCM-41@salen, HMS-C12, HMS-C12@salen, HMS-C16, and HMS-C16@salen (Fig. 8) present the features:

- for all unmodified silicas (MCM-41, HMS-C12, HMS-C16), type IV isotherms characteristic for the mesoporous materials have been obtained.[24,25] No hysteresis loop was observed for MCM-41, and this is a common feature for adsorbents having highly ordered mesopores, smaller than 4 nm width (Table 4).
- For HMS-C12 and HMS-C16, H2-type hysteresis loops are present and they are associated with slightly larger and less ordered mesoporous structures.

The pore volume and surface area of hemisalen functionalized silicas (MCM-41@salen, HMS-C12@salen, HMS-C16@salen) decrease dramatically in comparison with the parent MCM-41, HMS-C12, HMS-C16 silicas (Table 4). With the exception of HMS-C12@salen, which retains the framework mesoporosity and give a type IV isotherm (with capillary condensation step less visible), the other two silicas, MCM-41@salen and HMS-C16@salen, show type II isotherms and this fact could be attributed to pore blocking by salen ligands.

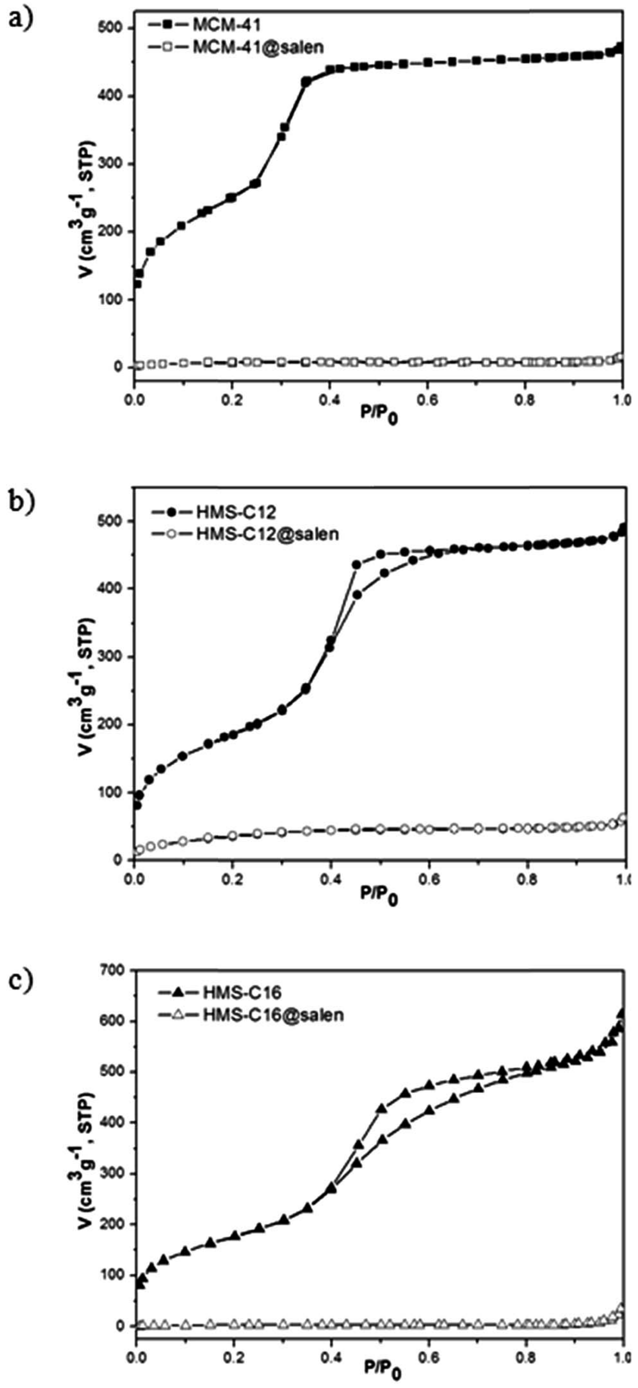

Fig. 8 Nitrogen adsorption–desorption isotherms of: (a) MCM-41, MCM-41@salen, (b) HMS-C12, HMS-C12@salen, and (c) HMS-C16, HMS-C16@salen.

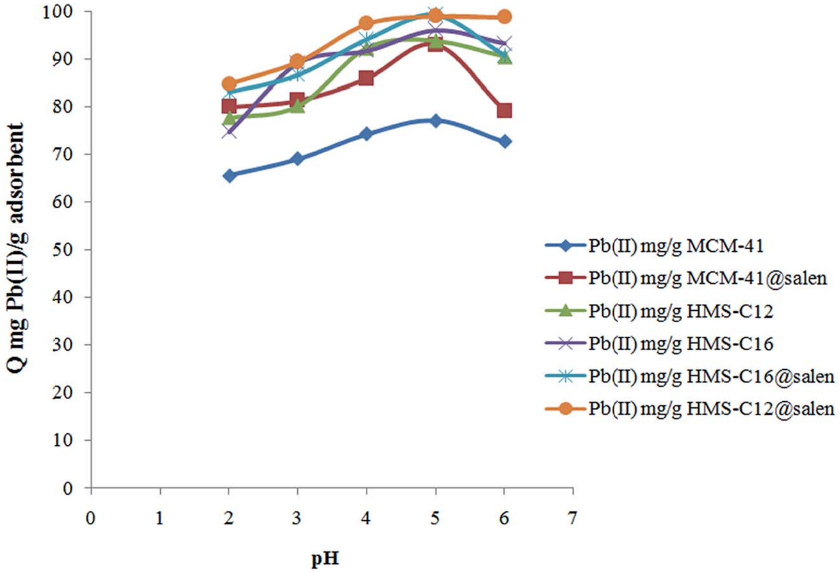

Fig. 9 Influence of pH solution on adsorption of Pb(II) (100 mg L^{-1} solutions) onto silicas.

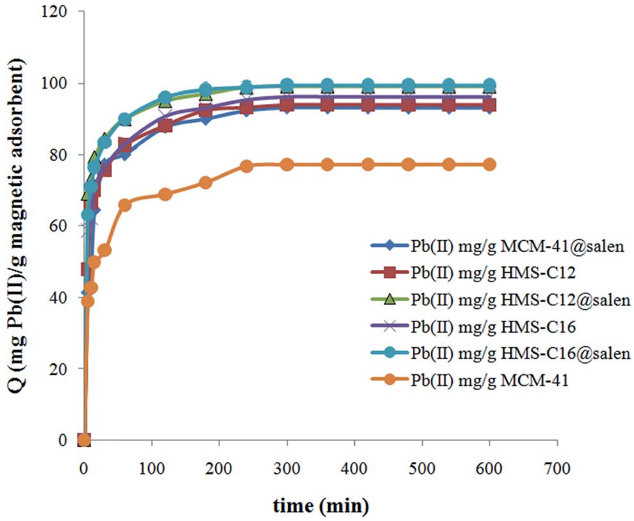

Fig. 10 Influence of contact time on Pb(II) adsorption onto synthesized silicas.

3.7. Pb(II) adsorption studies

Even at low concentration, Pb(II) damages tissues and organs such as kidneys, liver, reproductive and nervous system. Pb(II) has also indirect effects by inducing the production of reactive oxygen species (ROS) with negative consequences to cell macromolecules, proteins and polyunsaturated lipids.[26] The application of conventional removal methods such as chemical precipitation,[27] coagulation–flocculation,[28] ion exchange,[29] membrane filtration,[30] reverse osmosis,[31] electrochemical processes,[32] is limited by their high costs and inefficiency, in the case of low levels of Pb(II). Adsorption is one of the most used conventional process to remediate wastewater due to its simplicity, ease and rapid application and manipulation, the potential use of many natural materials (low cost) and synthetic materials as adsorbents.[33–39]

Mesoporous materials (MCM-41/HMS) have high surface area, narrow pore size distribution, tunable texture and surface properties, and a relative chemical inertness. These properties recommend their applications in sorption, catalysis, separation, sensors, hosts and numerous other fields.[40]

The MCM-41@salen, HMS-C12@salen, and HMS-C16@salen materials obtained by us have been used to uptake Pb(II) from synthetic aqueous systems and their sorption properties have been compared to those of parent MCM-41, HMS-C12, HMS-C16 mesoporous silicas.

3.7.1. Effect of initial pH on sorption capacity. The remediation of aqueous systems containing Pb(II) by adsorption depends primarily on the pH solution: the adsorbent surface charge, the ionic state of lead and also the ionization of the adsorbent functional groups are strongly affected by the pH solution.[41]

The influence of pH of solution in Pb(II) retention by MCM-41, MCM-41@salen, HMS-C12, HMS-C12@salen, HMS-C16 and HMS-C16@salen has been studied.

All the equilibrium tests were performed over the pH range of 2–6, by shaking 0.025 g of adsorbent with 25 mL of synthetic aqueous system of 100 mg L^{-1} Pb(II), at room temperature, for 24 hours and 150 rpm. The solutions were filtered and lead concentrations in the filtrate were determined by AAS, after reaching the equilibrium.

Fig. 9 presents the influence of pH of solution on sorption properties of our silica adsorbents, and their sorption capacity (Q) has been calculated as follows:

$$Q = \frac{\text{net amount of adsorbed Pb(II)}}{\text{the amount of adsorbent}} = \frac{(C_i - C_f) \times V}{m} \qquad (1)$$

where Q – Pb(II) uptake (mg g^{-1}); C_i – the concentration of contaminant in the initial solution (mg L^{-1}); C_f – the equilibrium concentration of contaminant (mg L^{-1}); m – the amount of adsorbent (g); V – the sample volume (L).

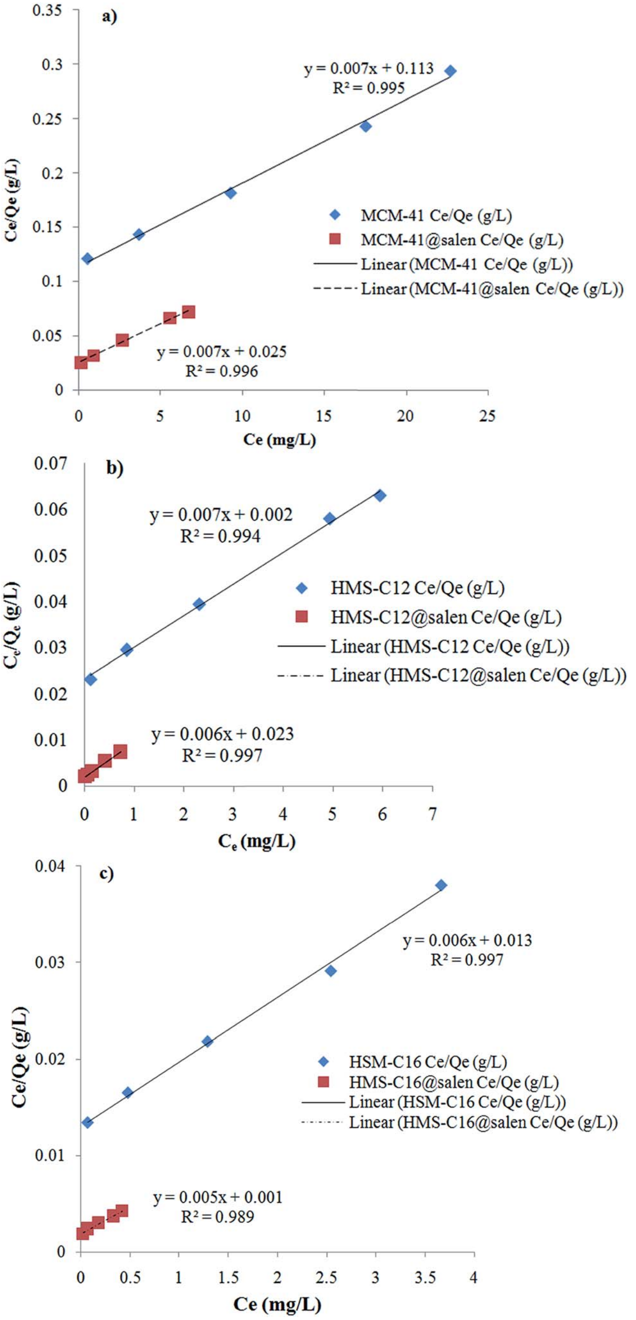

Fig. 11 Langmuir linearized isotherms for Pb(II) sorption onto (a) MCM-41, MCM-41@salen; (b) HMS-C12, HMS-C12@salen, (c) HMS-C16, HMS-C16@salen.

As can be observed (Fig. 9), the amount of Pb(II) retained by silicas increases with the increasing of the pH value. It reaches a maximum value at pH 5 and, then, it decreases slowly when pH solution changed from 5 to 6. At lower pH, a competition between Pb(II) ions and H^+ from solution for the adsorbents sites may occur. The experiments were conducted at a maximum value of 6 for pH solution. Beyond this pH the formation of lead hydroxo-species ($Pb(OH)^+$, $Pb(OH)_2{}^0$, and $Pb(OH)_3{}^-$) occurs and the precipitation of the Pb(II)-species can compete with sorption.

3.7.2. **Effect of contact time.** Fig. 10 illustrates the influence of the contact time on the Pb(II) adsorption from aqueous systems, for silica adsorbents.

The equilibrium was reached after 300 minutes and the sorption process of Pb(II) onto silica adsorbents can be considered a fast process. The large number of the available active sites of adsorbents determines the adsorption to proceed rapidly in the early stages of the process. With a gradual decrease in the number of active sites, the adsorption process rate decreases.

The experimental values of sorption capacities are: 77.31 mg Pb(II) per g MCM-41, 93.28 mg Pb(II) per g MCM-41@salen, 94.07 mg Pb(II) per g HMS-C12, 99.27 mg Pb(II) per g HMS-C12@salen, 96.34 mg Pb(II) per g HMS-C16, and 99.58 mg Pb(II) per g HMS-C16@salen. As expected, the functionalization of MCM-41, HMS-C12 and HMS-C16 with salen-type ligands has as a result a higher sorption capacity of functionalized silicas. This result can be due to the fact that N and O atoms, from salen ligands grafted on the silica surface of MCM-41@salen, HMS-C12@salen, and HMS-C16@salen adsorbents, are Lewis donors complementary to borderline Lewis acceptors Pb(II) ions and, therefore, the organofunctionalized silicas are more efficient in Pb(II) adsorption.

3.7.3. **Adsorption isotherms.** The adsorption isotherms represent mathematical expressions of the adsorbate–adsorbent interactions. These equations are useful to determine affinity of the sorbent, its surface properties, and also the sorption mechanism.[42] Langmuir, Freundlich, Temkin and Dubinin–Radushkevich isotherms are the most used to describe the adsorption equilibrium. The Langmuir isotherm represents an empirical equation that describes the process during the adsorption of contaminants/metal ions onto a fixed number of sorption sites.

Eqn (2) represents the linear expression of the Langmuir equation:[42]

$$\frac{C_e}{Q_e} = \frac{1}{Q_{\max}}C_e + \frac{1}{Q_{\max}K_L} \tag{2}$$

where Q_e is the amount of contaminant removed at equilibrium (mg g^{-1}); C_e is the equilibrium concentration of contaminant (mg L^{-1}); K_L is the Langmuir model parameter regarding energy of adsorption (L mg^{-1}) and $Q_{\max}$ states the maximum value of sorption capacity (mg g^{-1}).[42]

The Freundlich isotherm is frequently used to depict the sorption on heterogeneous surfaces, a process in which the concentration of adsorbate on the adsorbent surface increases with the adsorbate concentration and an infinite amount of adsorption can occur. The Freundlich model can be expressed as:

$$Q = K_F C_e{}^{1/n} \tag{3}$$

where K_F – constant for sorption capacity; n – Freundlich constant for sorption intensity.

The corresponding linear expression of Freundlich equation is:

$$\ln Q = \ln K_F + \frac{1}{n}\ln C_e \tag{4}$$

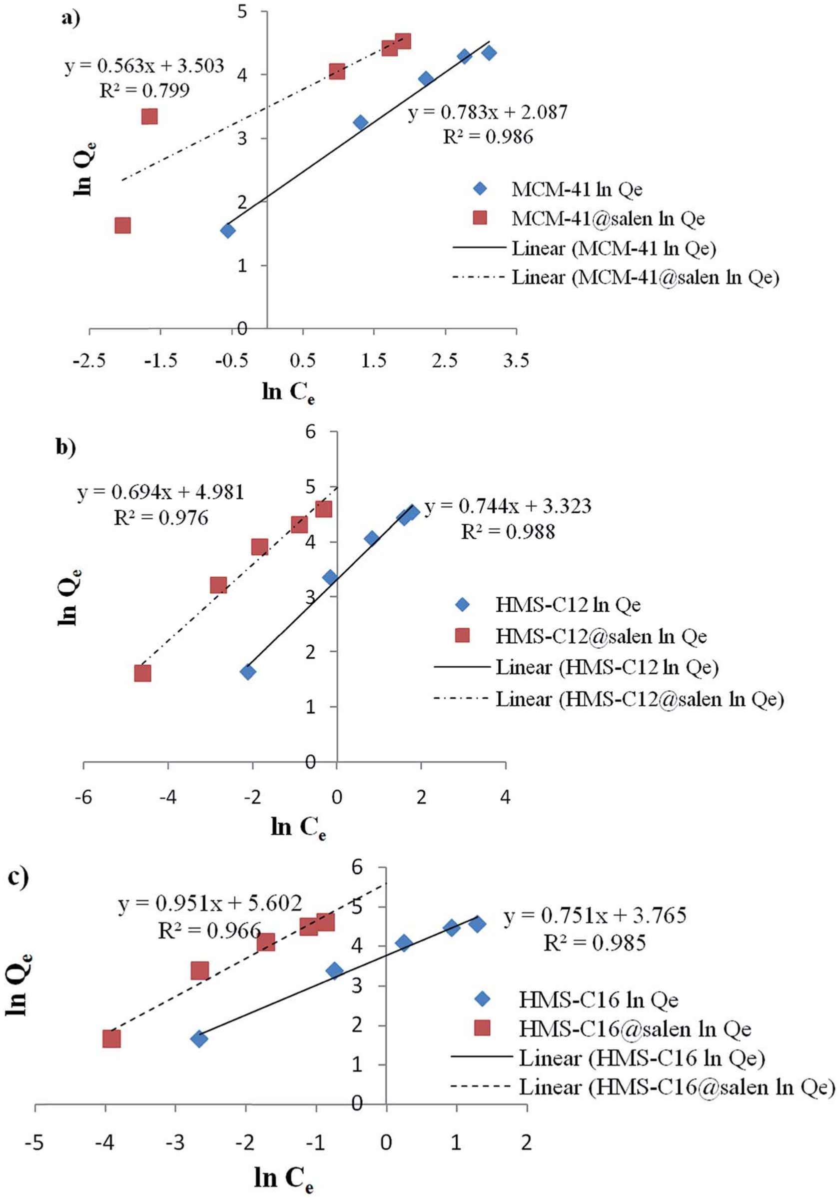

Fig. 12 Freundlich linearized isotherms for Pb(II) sorption onto (a) MCM-41, MCM-41@salen; (b) HMS-C12, HMS-C12@salen, (c) HMS-C16, HMS-C16@salen.

To study the thermodynamic equilibrium of Pb(II) sorption onto MCM-41, MCM-41@salen, HMS-C12, HMS-C12@salen, HMS-C16 and HMS-C16@salen, several experiments were performed with 5.28–100 mg L^{-1} Pb(II) solutions at room temperature and pH 5. Langmuir and Freundlich isotherm models for Pb(II) sorption onto MCM-41, MCM-41@salen, HMS-C12, HMS-C12@salen, HMS-C16 and HMS-C16@salen using linear regression are shown in Fig. 11 and 12.

Table 5 Langmuir and Freundlich sorption parameters

	Langmuir parameters			Freundlich parameters		
Sample	Q_{max} (mg g^{-1})	K_L (L mg^{-1})	R^2	K_F (mg g^{-1})	$1/n$	R^2
MCM-41	129.87	0.0677	0.9958	8.0679	0.7832	0.9860
MCM-41@salen	138.88	0.2845	0.9961	33.2249	0.5637	0.7995
HMS-C12	131.57	3.8000	0.9946	27.7573	0.7440	0.9883
HMS-C12@salen	144.92	0.2974	0.9978	145.7073	0.6948	0.9760
HMS-C16	149.25	0.5153	0.9970	43.1723	0.7517	0.9853
HMS-C16@salen	181.81	2.8947	0.9897	271.0220	0.9519	0.9660

Table 6 Pb(II) adsorption capacities (Langmuir model) of various sorbents from literature data

Adsorbent	Maximum adsorption capacity (mg g^{-1})	Reference
Chitosan-functionalized MCM-41 A	90.91	43
Large pore diameter MCM-41	174	44
ALG-MCM-41 (ALG – alginate)	140.84	45
MCM-41	57.7	46
Fe_3O_4@MCM-41-NH-oVan	155.71	47
Fe_3O_4@MCM-41-NH_2	126.14	47
Fe_3O_4@MCM-41	102.45	47
MCM-41	129.87	This work
MCM-41@salen	138.88	This work
HMS-C12	131.57	This work
HMS-C12@salen	144.92	This work
HMS-C16	149.25	This work
HMS-C16@salen	181.81	This work

The Langmuir and Freundlich constants and the calculated coefficients for Pb(II) sorption onto MCM-41, MCM-41@salen, HMS-C12, HMS-C12@salen, HMS-C16 and HMS-C16@salen are listed in Table 5.

It can be noticed that the correlation coefficients (R^2) are closer to 1 for the Langmuir isotherm. Consequently, the Langmuir isotherm model is more appropriate to describe the sorption process for all the studied adsorbents rather than Freundlich isotherm model.

The maximum values of adsorption capacity (Langmuir model) of our unmodified (MCM-41, HMS-C12 and HMS-C16) and organofunctionalized (MCM-41@salen, HMS-C12@salen and HMS-C16@salen) silicas are similar to the adsorption capacities of different Pb(II) adsorbents reported in literature (Table 6).

3.7.4. Adsorption kinetics.

Kinetic studies have been performed to determine the kinetic model that describes the Pb(II) remediation by MCM-41, MCM-41@salen, HMS-C12, HMS-C12@salen, HMS-C16 and HMS-C16@salen. The experimental data could be described by using three extensively used kinetic models: pseudo-first-order, pseudo-second-order and intraparticle diffusion.

According to the pseudo-first-order model, the rate of adsorption on sorbent is proportional to the number of free active sites of sorbent.[48] Lagergren eqn (5) is the mathematical expression of pseudo-first-order kinetic model:

$$\frac{\mathrm{d}Q_t}{\mathrm{d}t} = k_1(Q_e - Q_t) \tag{5}$$

where k_1 represents the constant rate of pseudo-first order sorption ($\min^{-1}$), and Q_e, Q_t symbolize the sorption capacities at equilibrium and at time t (mg g^{-1}). The linear form of this equation is:

$$\log(Q_e - Q_t) = \log Q_e - \frac{k_1}{2.303}t \tag{6}$$

where Q_e and Q_t represent the amounts of Pb(II) retained on adsorbent (mg g^{-1}) and k_1 is the first-order sorption rate constant ($\min^{-1}$). The slopes and intercepts of plots of $\log(Q_e - Q_t)$ *versus* t have been used to calculate k_1 and the correlation coefficient R^2 (Fig. 13a–c).

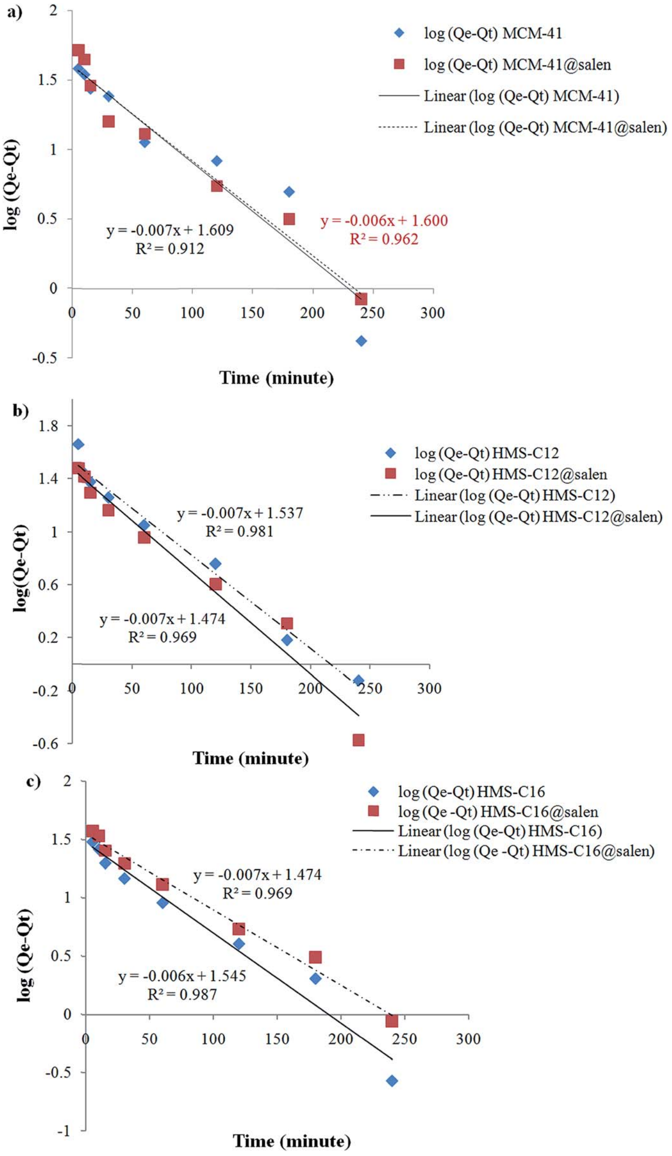

Fig. 13 Pseudo-first order sorption kinetics of Pb(II) onto (a) MCM-41, MCM-41@salen; (b) HMS-C12, HMS-C12@salen; (c) HMS-C16 and HMS-C16@salen.

The pseudo-second-order kinetic model is mathematically summarised as Ho eqn (7):

$$\frac{t}{Q_t} = \frac{1}{k_2 {Q_e}^2} + \frac{t}{Q_e} \tag{7}$$

where k_2 depicts the rate constant of second-order adsorption (g mg^{-1} $\min^{-1}$).[49] The line plots t/Q_t against t were used for the parameters of the pseudo-second-order kinetic model (Fig. 14a–c).

The intraparticle diffusion model is depicted by the mathematical equation:

$$Q_t = k_i t^{0.5} \tag{8}$$

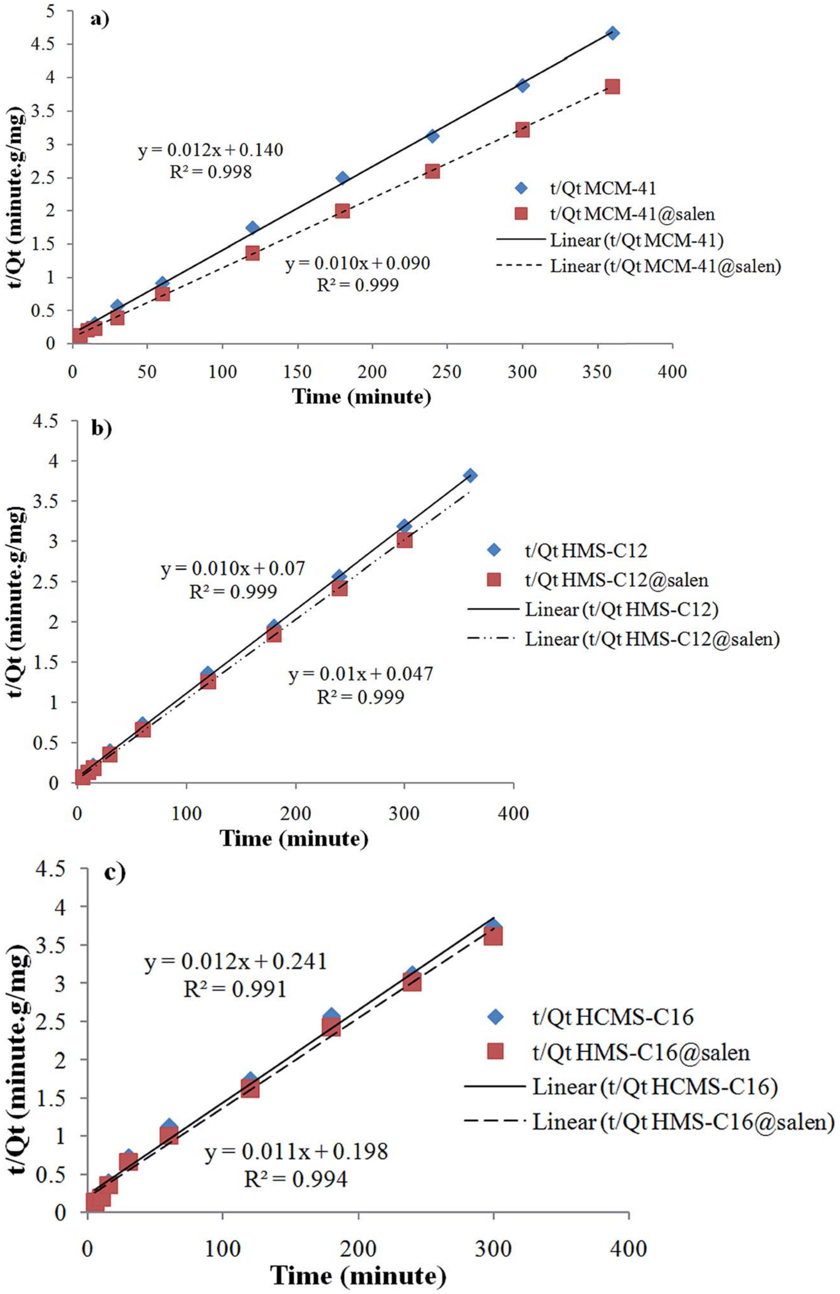

Fig. 14 Pseudo-second order sorption kinetics of Pb(II) onto (a) MCM-41, MCM-41@salen; (b) HMS-C12, HMS-C12@salen; (c) HMS-C16 and HMS-C16@salen.

where k_i represents the intraparticle diffusion rate constant (mg g^{-1} $min^{-0.5}$). The graphic representations of Q_t *versus* $t^{0.5}$ (Fig. 15) have been used to evaluate the k_i value.

Since the plots for all six silicas are not linear and they do not pass through the origin, the intraparticle diffusion can not be considered the rate-limiting step for the Pb(II) sorption onto MCM-41, MCM-41@salen, HMS-C12, HMS-C12@salen, HMS-C16 and HMS-C16@salen samples. The plots are multilinear with two or three distinct regions. Thus, two or three different kinetic mechanisms are involved. According to literature data, it can be supposed that the initial curved region correlates with the external surface uptake, the second stage represents a gradual uptake reflecting intraparticle diffusion as the rate limiting step and the final plateau region shows the sorption equilibrium.[50]

Kinetic parameters show a good correlation with experimental kinetic values for pseudo-second order model ($R^2 >$ 0.991 for all six adsorbents – Table 7). Consequently, the chemisorption is considered to be the rate-limiting stage.[49]

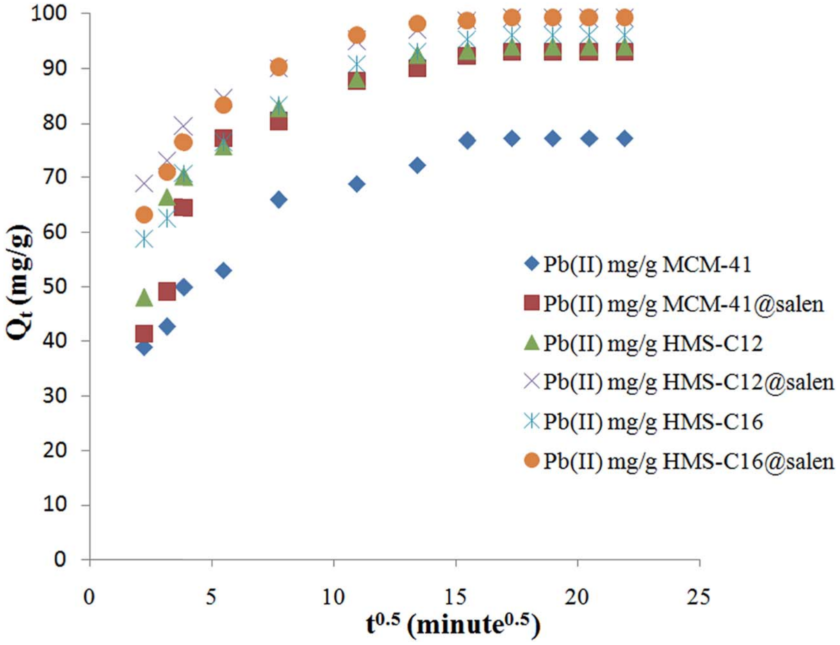

Fig. 15 Intraparticle diffusion sorption kinetics of Pb(II) onto MCM-41, MCM-41@salen, HMS-C12, HMS-C12@salen, HMS-C16 and HMS-C16@salen.

Table 7 The kinetic model parameters for Pb(II) sorption onto MCM-41, MCM-41@salen, HMS-C12, HMS-C12@salen, HMS-C16 and HMS-C16@salen samples

	Pseudo-first order model		Pseudo-second order model	
Sample	k_1 (min^{-1})	R^2	k_2 (g mg^{-1} min^{-1})	R^2
MCM-41	1.6121×10^{-2}	0.9124	1.1267×10^{-3}	0.9989
MCM-41@salen	1.3818×10^{-2}	0.9620	1.2222×10^{-3}	0.9998
HMS-C12	1.7963×10^{-2}	0.9694	1.5451×10^{-3}	0.9998
HMS-C12@salen	1.6351×10^{-2}	0.9819	2.1277×10^{-3}	0.9998
HMS-C16	1.4969×10^{-2}	0.9875	0.6072×10^{-3}	0.9913
HMS-C16@salen	1.7963×10^{-2}	0.9694	0.6896×10^{-3}	0.9943

4. Conclusions

Organofunctionalized silicas, MCM-41@salen, HMS-C12@salen and HMS-C16@salen, obtained from parent mesoporous silicas: MCM-41, HMS-C12 and HMS-C16 (CTAB, dodecylamine and hexadecylamine, as templates) have been prepared and tested for the ability to adsorb Pb(II) from aqueous systems.

Even though the framework mesoporosity partially decreased as a consequence of grafting the salen ligands onto the silica surface, the coordinative sites still remained accessible for binding heavy metal ions.

Kinetic studies have been performed to determine the kinetic model that describes the Pb(II) sorption onto MCM-41, MCM-41@salen, HMS-C12, HMS-C12@salen, HMS-C16 and HMS-C16@salen. The lead adsorption was well fitted by a pseudo second-order kinetic model ($R^2 > 0.991$ for all six adsorbents) and a Langmuir isotherm model has been more appropriate to describe the sorption process for all the studied adsorbents rather than Freundlich isotherm model.

The values of Langmuir sorption capacity suggest that the obtained Schiff base-functionalized mesoporous silicas are relevant materials for the removal and recovery of Pb(II) and also could be used as effective adsorbents of Pb(II) from wastewaters.

Conflicts of interest

There are no conflicts to declare.

Acknowledgements

Financial support by the Ministry of National Education – Executive Unit for Financing Higher Education, Research and Development and Innovation (MEN – UEFISCDI), PNII – PCCA No. 92/2014 and Romanian Ministry of European Funds through the Financial Agreement POSDRU/159/1.5/S/132395 is gratefully acknowledged.

References

1 P. K. Jal, S. Patel and B. K. Mishra, *Talanta*, 2004, **62**, 1005–1028.
2 A. Taguchi and F. Schüth, *Microporous Mesoporous Mater.*, 2005, **77**, 1–45.
3 K. Ariga, A. Vinu, J. P. Hill and T. Mori, *Coord. Chem. Rev.*, 2007, **251**, 2562–2591.
4 B. Samiey, C.-H. Cheng and J. Wu, *Materials*, 2014, **7**, 673–726.
5 H. Yoshitake, *J. Mater. Chem.*, 2010, **20**, 4537–4550.

6 H. Yoshitake, *New J. Chem.*, 2005, **29**, 1107–1117.

7 A. Choplin and F. Quignard, *Coord. Chem. Rev.*, 1998, **178–180**, 1679–1702.

8 K. Parida, K. Gopal Mishra and S. K. Dash, *Ind. Eng. Chem. Res.*, 2012, **51**, 2235–2246.

9 T. Yokoi, Y. Kubota and T. Tatsumi, *Appl. Catal., A*, 2012, **421–422**, 14–37.

10 E. M. Soliman, M. E. Mahmoud and S. A. Ahmed, *Talanta*, 2001, **54**, 243–253.

11 G.-J. Kim and J.-H. Shin, *Tetrahedron Lett.*, 1999, **40**, 6827–6830.

12 A. R. Sarkar, P. K. Datta and M. Sarkar, *Talanta*, 1996, **43**, 1857–1862.

13 V. Parvulescu, M. Mureseanu, A. Reiss, R. Ene and S.-H. Suh, *Rev. Roum. Chim.*, 2010, **55**, 1001–1008.

14 M. Mureseanu, A. Reiss, I. Stefanescu, E. David, V. Parvulescu, G. Renard and V. Hulea, *Chemosphere*, 2008, **73**, 1499–1504.

15 L. Dolatyari, M. R. Yaftian and S. Rostamnia, *J. Environ. Manage.*, 2016, **169**, 8–17.

16 X. Chen, A. Yamaguchi, M. Namekawa, T. Kamijo, N. Teramae and A. Tong, *Anal. Chim. Acta*, 2011, **696**, 94–100.

17 L. Gao, Y. Wang, J. Wang, L. Huang, L. Shi, X. Fan, Z. Zou, T. Yu, M. Zhu and Z. Li, *Inorg. Chem.*, 2006, **45**, 6844–6850.

18 K. S. Abou-El-Sherbini, I. M. M. Kenawy, M. A. Hamed, R. M. Issa and R. Elmorsi, *Talanta*, 2002, **58**, 289–300.

19 V. S.-Y. Lin, C.-Y. Lai, S. Jeftinija and D. M. Jeftinija, *US Pat.*, 2009/0252811, 2009.

20 P. T. Tanev and T. J. Pinnavaia, *Chem. Mater.*, 1996, **8**, 2068–2079.

21 V. Meynen, P. Cool and E. F. Vansant, *Microporous Mesoporous Mater.*, 2009, **125**, 170–223.

22 D. Banham, F. Feng, J. Burt, E. Alsrayheen and V. Birss, *Carbon*, 2010, **48**, 1056–1063.

23 D. Banham, F. Feng, K. Pei, S. Ye and V. Birss, *J. Mater. Chem. A*, 2013, **1**, 2812–2820.

24 K. S. W. Sing, D. H. Everett, R. A. W. Haul, L. Moscou, R. A. Pierotti, J. Rouquerol and T. Siemieniewska, *Pure Appl. Chem.*, 1985, **57**(4), 603–619.

25 M. Thommes, K. Kaneko, A. V. Neimark, J. P. Olivier, F. Rodriguez-Reinoso, J. Rouquerol and K. S. W. Sing, *Pure Appl. Chem.*, 2015, **87**(9–10), 1051–1069.

26 M. Cabral, A. Toure, G. Garçon, C. Diop, S. Bouhsina, D. Dewaele, F. Cazier, D. Courcot, A. Tall-Dia, P. Shirali, A. Diouf, M. Fall and A. Verdin, *Environ. Pollut.*, 2015, **206**, 247–255.

27 G. Németh, L. Mlinárik and Á. Török, *J. Afr. Earth Sci.*, 2016, **122**, 98–106.

28 F. M. Pang, P. Kumar, T. T. Teng, A. K. M. Omar and K. L. Wasewar, *J. Taiwan Inst. Chem. Eng.*, 2011, **42**, 809–815.

29 D. S. Stefan and I. Meghea, *C. R. Chim.*, 2014, **17**, 496–502.

30 N. Abdullah, R. J. Gohari, N. Yusof, A. F. Ismail, J. Juhana, W. J. Lau and T. Matsuura, *Chem. Eng. J.*, 2016, **289**, 28–37.

31 K. Chon, J. Cho, S. J. Kim and A. Jang, *Chemosphere*, 2014, **117**, 20–26.

32 S. Li, Y. Wei, Y. Kong, Y. Tao, C. Yao and R. Zhou, *Synth. Met.*, 2015, **199**, 45–50.

33 Y. Li, R. Zhang, X. Tian, C. Yang and Z. Zhou, *Appl. Surf. Sci.*, 2016, **369**, 11–18.

34 A. Behbahani, H. Eghbali, M. Ardjmand, M. M. M. Noufal, H. C. Williamson and O. Sayar, *J. Environ. Chem. Eng.*, 2016, **4**, 398–404.

35 M. E. Mahmoud, N. A. Fekry and M. M. A. El-Latif, *Chem. Eng. J.*, 2016, **304**, 679–691.

36 G. Zhou, C. Liu, L. Chu, Y. Tang and S. Luo, *Bioresour. Technol.*, 2016, **219**, 451–457.

37 Y. Zhu, D. Jiang, D. Sun, Y. Yan and C. Li, *J. Environ. Chem. Eng.*, 2016, **4**, 3570–3579.

38 I. Lakhdhar, D. Belosinschi, P. Mangin and B. Chabot, *J. Environ. Chem. Eng.*, 2016, **4**, 3159–3169.

39 G. Zhou, J. Luo, C. Liu, L. Chu, J. Ma, Y. Tang, Z. Zeng and S. Luo, *Water Res.*, 2016, **89**, 151–160.

40 M. R. El-Naggar, R. F. Aglan and M. S. Sayed, *J. Environ. Chem. Eng.*, 2013, **1**, 516–525.

41 F. Chen, M. Hong, W. You, C. Li and Y. Yu, *Appl. Surf. Sci.*, 2015, **357**, 856–865.

42 M. Rashid and F. K. Lutfullah, *Journal of Water Process Engineering*, 2014, **3**, 53–61.

43 Y. Guo, D. Liu, Y. Zhao, B. Gong, Y. Guo and W. Huang, *J. Taiwan Inst. Chem. Eng.*, 2017, **71**, 537–545.

44 S. A. Idris, C. M. Davidson, C. McManamon, M. A. Morris, P. Anderson and L. T. Gibson, *J. Hazard. Mater.*, 2011, **185**, 898–904.

45 H. Tavakoli, H. Sepehrian and R. Cheraghali, *J. Taiwan Inst. Chem. Eng.*, 2013, **44**, 343–348.

46 A. Heidari, H. Younesi and Z. Mehraban, *Chem. Eng. J.*, 2009, **153**, 70–79.

47 D. C. Culita, C. M. Simonescu, R.-E. Patescu, M. Dragne, N. Stanica and O. Oprea, *J. Solid State Chem.*, 2016, **238**, 211–220.

48 T. Yousefi, S. Yavarpour, S. H. Mousavi, M. Torab-Mostaedi, R. Davarkhah and H. G. Mobtaker, *Process Saf. Environ. Prot.*, 2015, **98**, 211–220.

49 Y. S. Ho and G. McKay, *Trans. Inst. Chem. Eng.*, 1998, **76**, 332–340.

50 R. S. Popuri, Y. Vijaya, V. M. Boddu and K. Abburi, *Bioresour. Technol.*, 2009, **100**, 194–199.